Available online at www.sciencedirect.com
ScienceDirect
Bioorganic & Medicinal Chemistry 15 (2007) 2935–2943
Bioorganic & Medicinal Chemistry

Structure–activity based study of the Smac-binding pocket within the BIR3 domain of XIAP

Aislyn D. Wist,[a,*,†] Lichuan Gu,[b] Stefan J. Riedl,[b,‡] Yigong Shi[b] and George L. McLendon[a,*,§]

[a]*Department of Chemistry, Princeton University, Princeton, NJ 08544, USA*
[b]*Department of Molecular Biology, Princeton University, Princeton, NJ 08544, USA*

Received 19 December 2006; revised 31 January 2007; accepted 8 February 2007
Available online 11 February 2007

Abstract—A small series of peptide mimics was designed and synthesized to contain a heterocyclic ring in place of the potentially labile N-terminal peptide bond of the tetrapeptide containing the Smac-XIAP-binding motif. Two Smac mimics were shown to bind to the BIR3 domain of XIAP with moderate affinity and one displayed increased activity in cells relative to the Smac peptides. The structures of BIR3-XIAP in complex with a Smac peptide and a peptide mimic were solved and analyzed to elucidate the structure–activity relationship surrounding the Smac-binding domain within BIR3-XIAP.

1. Introduction

Apoptosis plays a major role in maintaining the balance between cell proliferation and cell death. Imbalances in the apoptotic pathway are linked to several different types of diseases.[1–3] For instance, it is generally recognized that in many types of cancer the apoptotic pathway is inactivated in some way. One mechanism by which this occurs is the upregulation of anti-apoptotic proteins, such as the IAP (inhibitor of apoptosis) family of proteins, which prevent apoptosis from occurring by sequestering caspases (cysteine-aspartic acid protease).[4,5]

An IAP family member, XIAP (X-linked IAP), functions by directly binding and inhibiting the active subunit of caspase-9, an initiation caspase in the mitochondrial cell death pathway.[2] Upon its release from the mitochondria, Smac/DIABLO (the second mitochondrial activator of apoptosis[6]/direct IAP-binding protein with low pI)[7] binds to XIAP using the same binding motif as caspase-9, thus causing its displacement.[8,9] Once released from XIAP, caspase-9 can activate downstream caspases (−3 and −7) which go on to destroy cellular targets and promote cell death. However, due to the high level of XIAP present in many types of cancer cells,[5,10] the amount of Smac released from the mitochondria may not be sufficient to overcome the inhibitory effect of XIAP on caspase-9; thus tipping the balance toward life rather than programmed cell death. The anti-apoptotic behavior of XIAP and the critical role it plays in the apoptotic program makes the Smac-XIAP interaction an important drug target.

Molecules able to mimic Smac could counter an excess of XIAP, restoring the ability of the apoptotic machinery to fully execute programmed cell death. Typically it is a greater challenge to target a protein–protein interaction compared to an enzyme active site with a small molecule, because large and diverse surface areas are generally involved and drug molecules are usually low molecular weight.[11,12] The design of small molecules to target the Smac-XIAP interaction is facilitated by the structural data[13,14] which revealed that the interaction consists primarily of the N-terminal tetrapeptide of Smac binding to a surface groove on the BIR3 (baculovirus IAP repeat) domain of XIAP. However, since the target is a protein–protein interaction, the structure

Keywords: XIAP; Smac; Peptide mimetics; Apoptosis; Rational design; Oxazole.
* Corresponding authors. Tel.: +1 919 684 4510; fax: +1 919 684 8503; e-mail addresses: aislyn.wist@mssm.edu; george.mclendon@duke.edu
† Present address: Department of Pharmacology and Biological Chemistry, Mount Sinai School of Medicine, New York, NY 10029, USA.
‡ Present address: Burnham Institute for Medical Research, La Jolla, CA 10901, USA.
§ Present address: Department of Chemistry, 104 Allen Building, Duke University, Durham, NC 27708, USA.

0968-0896/$ - see front matter © 2007 Elsevier Ltd. All rights reserved.
doi:10.1016/j.bmc.2007.02.010

activity relationship is particularly convoluted by structural dynamics contributed by both the small molecule and the flexible protein-binding site. In order to elucidate the structure activity relationship, it is necessary to capture the molecular movements during binding.

In the present study, novel Smac mimics were designed and synthesized to contain a heterocycle in place of the N-terminal bond. While there are several studies which produced partially non-peptidic Smac mimics,[15–18] this is the first study to present Smac mimics where the N-terminal peptide bond is modified to a non-peptidic structure and binding affinity for BIR3-XIAP is retained. From a drug design perspective, it is important to produce a completely non-peptidic molecule to maximize bioavailability and stability properties. This has been a challenge with this particular target due to the small hydrophobic pocket and intricate hydrogen bonding network involved with the binding of the N-terminal segment of the Smac peptide/mimic. In order to understand the structural implications of this modification, the crystal structures of Smac, a peptide ligand or a peptide mimic bound to the BIR3 domain of XIAP (BIR3-XIAP), are presented and analyzed for conformational changes that occur within the binding pocket and in the respective ligands. The structural basis for the differences in binding affinity for the Smac mimic compared to the peptides is described. The biological activity of the peptide mimic and peptides is compared in cell viability assays.

2. Results and discussion

2.1. Design and synthesis of Smac mimics

The Smac mimic chosen for this structural study was designed based on a tetrapeptide (AVPW) that has been shown to bind to BIR3-XIAP with high affinity.[19] This previously published study mapped out the residues that are critical for binding to BIR3-XIAP by systematically substituting the amino acids in the N-terminal region of Smac. Specifically, modification of the position 1 Ala dramatically reduced binding affinity; whereas, the position 4 Ile was more amenable to modification and switching to aromatic residues such as Phe and Trp increased binding affinity for BIR3-XIAP. In order to reduce the peptidic character of the Smac mimic, one peptide bond was replaced with an oxazole ring to produce a series of Smac mimics (Table 1) with the anticipation that such modification would render the molecule more 'drug-like' by increasing its uptake and stability in a cellular context.

The heterocycle insertion caused a reduction in binding affinity, but not as drastically as other modifications to the first peptide bond, such as N-methylation.[19] AoxSPW bound to BIR3-XIAP with an affinity of 30 μM (Table 1), while AVPF and AVPI bind with 0.5, 0.04 μM, respectively. In order to understand the structural differences that attributed to the difference in binding affinity, AoxSPW (Table 1, entry 2) was co-crystallized with BIR3-XIAP to yield X-ray quality crystals and the structure of the bound complex was solved at 2.8 Å resolution. The structure of AVPF bound to BIR3-XIAP was also solved. These structures are compared to the Smac:BIR3-XIAP structure (PDB ID: IG3F).[14] Images rendered using PyMol[20] from the X-ray crystallographic data of AVPF or AoxSPW bound to BIR3-XIAP are shown in Figure 1a–c.

2.2. Comparison of the hydrogen-bonding networks

In comparing the crystal structures of AVPI, AVPF, and AoxSPW bound to BIR3-XIAP, it is apparent that the hydrogen-bonding network has changed in the AoxSPW structure relative to the peptide/protein structures. There are five hydrogen bonds (depicted by red dotted lines in Figure 1) to BIR3 in the AoxSPW structure and seven hydrogen bonds to BIR3 each in the AVPI and AVPF structures. The terminal amine of AoxSPW maintains two hydrogen bonds with the carboxylic acid of BIR3 E314, but loses one with Q319 that is present in the AVPI and AVPF structures. Two hydrogen bonds involving the N-terminal peptide bond are present, but shifted around slightly in the AoxSPW relative to the AVPI and AVPF structures. The position of the oxazole ring causes a loss of the hydrogen bond with the indole N–H of W323. However, the carbonyl oxygen between the proline and the oxazole ring of AoxSPW forms a new hydrogen bond with the hydroxide proton of T308, which is not present in the AVPI and AVPF structures. A backbone hydrogen bond formed between the amide proton in the second peptide bond (P–I or P–F) and BIR3 G306 is not present in the AoxSPW structure due to the orientation of AoxSPW in the pocket. Overall, there is a loss of three hydrogen bonds and a gain of one in the AoxSPW structure with respect to the hydrogen bonds in the AVPI and AVPF structures, which may partially account for the relative loss of binding affinity with AoxSPW for BIR3-XIAP.

In addition to the hydrogen bonds, there are hydrophobic interactions between AoxSPW and BIR3-XIAP. Similar to AVPI and AVPF, the A1 β-methyl group is buried in the small hydrophobic pocket in BIR3 near W310. The methylene chains of BIR3 K297 and K299 interact with the indole ring of W4 in AoxSPW, in a similar manner as F4 of AVPF. The distance between the heteroatoms in the oxazole ring in the nearby BIR3 residues, Q319 (sidechain) and T308 (backbone), indicates there are also dipole–dipole interactions, which may partially compensate for missing hydrogen bonds. Taken together, it appears that several intramolecular hydrogen bonds of BIR3 were interchanged in order to accommodate AoxSPW into the binding pocket, while maximizing hydrophobic and dipole–dipole interactions.

2.3. Comparison of ligand conformations

The positions of bound ligand were compared by overlaying each of the bound structures with respect to the residue positions in XIAP-BIR3 using XtalView. This analysis allowed for further explanation of the relative

Table 1. The position 1, 2 peptide bond in N-terminal Smac tetrapeptide was replaced by an oxazole

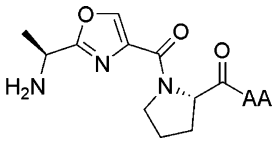

Entry	Smac mimic	AA	K_D ± std dev[a] (μM)	Relative to AVPI[b]
1	AoxSPF	Phe	11 ± 3	50 ± 14
2	AoxSPW	Trp	30 ± 12	70 ± 8
3	AoxSPY	Tyr	120 ± 60	170 ± 80
4	AoxSPI	Ile	300 ± 60	400

The binding affinity for BIR3-XIAP and the binding affinity relative to AVPI are shown.
[a] Standard deviations for three or more separate experiments.
[b] Relative to the value for AVPI during each individual assay was calculated by dividing the K_D of the Smac mimic by the K_D of AVPI.

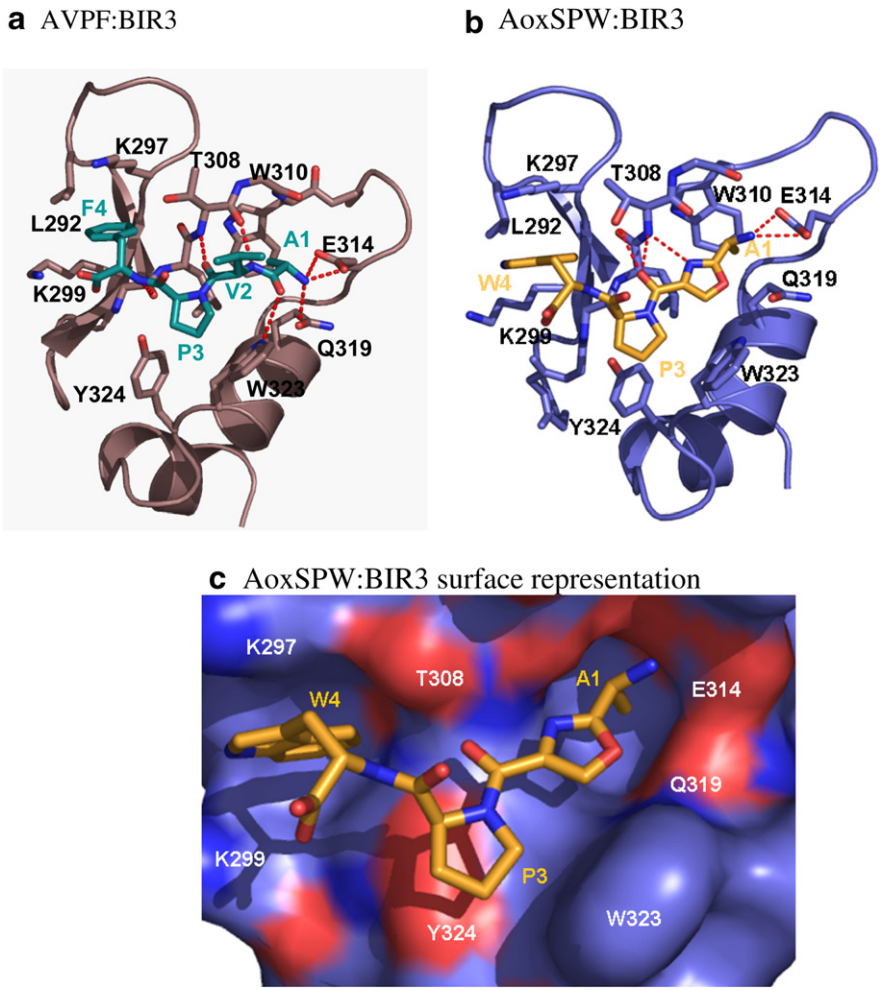

Figure 1. Image rendered from crystal structure of the (a) AVPF (green) bound to BIR3-XIAP (mauve) and (b) AoxSPW (gold) bound to BIR3-XIAP (blue). Hydrogen bonds are shown as red dotted lines. Note that a strand of a β-sheet (between G306 and T308) is shown in detail instead of a cartoon arrow for clarity. (c) Surface depiction of AoxSPW (gold) bound to BIR3-XIAP (blue). Red and blue represent oxygen and nitrogen, respectively. Images were rendered using PyMol.[20]

binding affinities. Overlaid images of the bound ligands (AVPI overlaid with AoxSPW and AVPI overlaid with AVPF) derived from the respective superimposed BIR3-XIAP structures are shown in Figure 2. The ligands are in the bound conformations and shown with several surrounding BIR3-XIAP residues. The oxazole, an aromatic, planar ring, is more sterically constrained than an amide bond and is therefore expected to induce some significant shifts in atom positioning relative to AVPI. Indeed, from the perspective in the plane of the oxazole ring, the atoms are shifted significantly (Fig. 2a). The N-terminal amines are 0.80 Å apart, causing the AoxSPW amine to form two hydrogen bonds with BIR3-XIAP instead of three. The alanine β-methyl

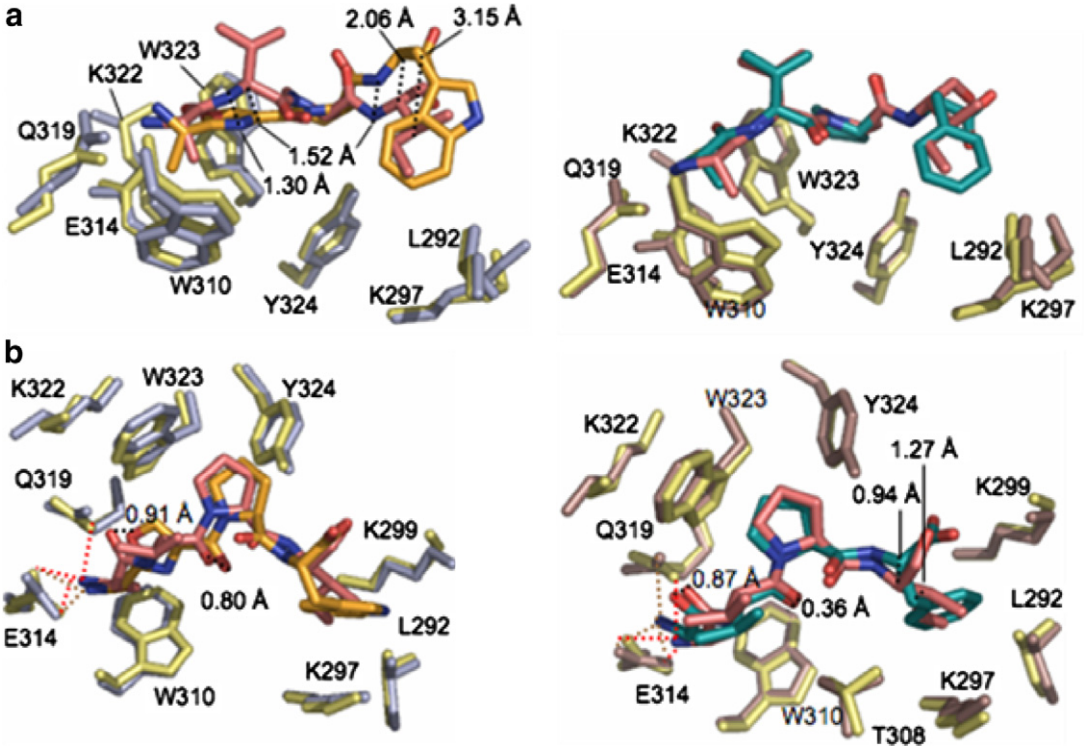

Figure 2. Images of the superimposed conformations of (*left panel*) AoxSPW (gold) and AVPI (pink), and (*right panel*) AVPI (pink) and AVPF (turquoise). (a) Perspective from the plane perpendicular to the plane of the proline ring. (b) Perspective from the plane of the proline ring. Surrounding BIR3-XIAP residues are shown from each structure: AoxSPW (blue), AVPI (yellow), and AVPF (mauve). Several distances between parallel atoms are labeled as dashed black lines. Hydrogen bonds formed by AVPI are shown as dashed red lines and by AVPF or AoxSPW as dashed brown lines. Elements are shown as follows: C is gold/pink, O is red, N is blue. Images were rendered as sticks using PyMol and the superimposed coordinates were produced using XtalView.

groups are 1.03 Å apart (measurement not shown), most likely causing a loss in hydrophobic interaction with BIR3-XIAP for AoxSPW relative to AVPI. The combination of orientation of the alanine β-methyl and the amine to retain some hydrophobic and hydrogen bonding interactions and the steric constraint of the oxazole causes the Trp-containing portion of AoxSPW to buckle outward relative to AVPI. This is highlighted by the 3.15 Å distance between the β-methyls of Trp and Ile from AoxSPW and AVPI, respectively (Fig. 2a). In contrast, the two peptide ligands, AVPI and AVPF, map relatively well onto each other in the binding pocket (Fig. 2b). The largest displacement is between the β-methyls, which are 1.27 Å apart. The movement is most likely caused by the insertion of the AVPF phenyl ring between the two nearby BIR3 lysines. The hydrophobic interaction is less effective with the branched isobutyl group of AVPI, which is more sterically hindered and less able to properly insert between the two Lys methylene chains.

There are some atoms that map relatively well between AVPI and AoxSPW, when viewed from the perspective perpendicular to the plane of the oxazole ring (Fig. 2a). However, even seemingly small movements (<1 Å) correspond to changes in interactions that potentially contribute to overall binding affinity. For example, the oxazole ring oxygen and the AVPI carbonyl oxygen are relatively close in space (0.91 Å apart); however, the AVPI oxygen donates a hydrogen bond to the BIR3 indole ring amine, whereas the oxazole oxygen does not. Such small movements may be able to disrupt hydrogen bonding since the Smac mimic has access to a more limited conformational space compared to AVPI, due to the increased steric constraint of the oxazole relative to an amide bond. On the other hand, BIR3-XIAP residues are shifted to allow for some new contacts in the AoxSPW structure. For example, the carbonyl groups of AVPI and AoxSPW (between Val and Pro and the oxazole and Pro) are in close proximity (0.78 Å), yet the AoxSPW carbonyl participates in an extra hydrogen bond with BIR3 T308; therefore movement of BIR3 T308 group was most likely responsible for this interaction.

2.4. Comparison of BIR3 residue positioning

The protein is not static and residue and/or backbone movements in the protein also contribute to the overall binding. From a visual comparison of the positions and distances in the crystal structures, it is apparent that the protein is displaced in the AoxSPW structure relative to the AVPI structure. For example, G304 through L307 participate in β-sheet formation in the AoxSPW structure while this β-sheet is from G306 through T308 in the AVPI structure; this causes the nearby loop to be longer in the AVPI structure (not shown in images). Thus, several intramolecular hydrogen bonds of BIR3 were switched around in order to accommodate AoxSPW into the binding pocket.

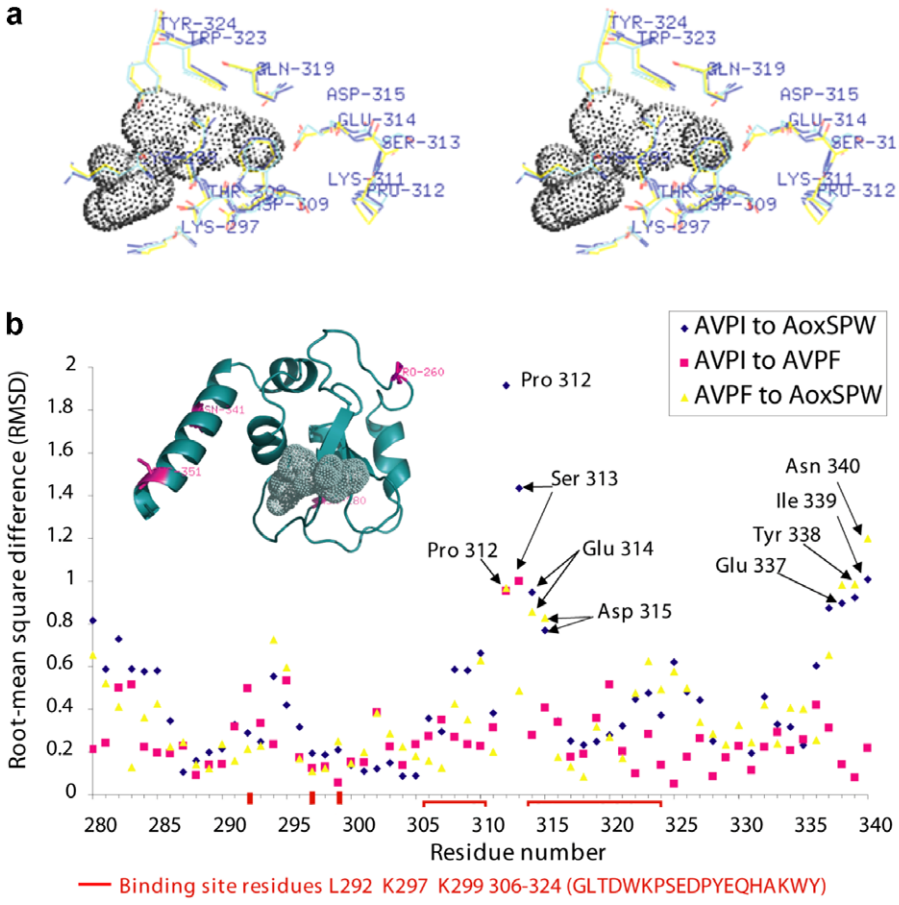

Figure 3. (a) Stereo view of the superimposed conformations of the binding site residues of BIR3-XIAP in the AoxSPW (cyan), AVPI (yellow) or AVPF (blue–gray) bound states. The space that the ligand occupies is represented as dots, rendered using AoxSPW. (b) Plot of the root-mean-square difference value for residue positions in the structures of AVPI, AVPF, and AoxSPW bound to BIR3-XIAP. The values for the AVPI structure superimposed on the AoxSPW structure are blue, AVPI superimposed on AVPF are pink and AVPF to AoxSPW are yellow. The residues closest to the binding site are highlighted in red. The RMSD values were calculated for residues 280–340 using XtalView. The cartoon image of AoxSPW:BIR3 structure with AoxSPW in dots is displayed for residue number reference (rendered in Pymol.).

There are other more subtle spatial shifts that are notable between the three structures, depicted in the overlay images in Figure 3a, which contains several views of the superimposed BIR3-XIAP structures from the AVPI-, AVPF-, and AoxSPW-bound states. To examine the movement of each residue more closely, root-mean-square difference (RMSD) value for the movement of each residue was calculated for BIR3 residues in the AVPI structure with respect to the AoxSPW structure, the AVPF structure with respect to the AoxSPW structure, and the AVPI structure with respect to the AVPF structure. The three sets of values were plotted in on the same axes, shown in Figure 3b. Proteins are not static in solution, some movement is 'natural;' however, larger displacements (beyond what is natural RMSD >∼0.4) were detected and were most likely due to the ligand binding. Examples of residues that are displaced in the AoxSPW structure include Pro 312, Ser 313, Glu 314, and Asp 315. Not all of these residues have a direct interaction with the ligand, such as a hydrogen bond or van der Waals. They are most likely displaced in a compensatory affect to accommodate the ligand in the binding pocket. Closer examination of the RMSD values reveals that there may be a distal effect of the AoxSPW ligand binding. There is high deviation near BIR3-XIAP 337–340 which is most likely due to an artifact caused by the relative disorder in this part of the protein, which is an α-helix that juts out and has relatively little interaction with the rest of the protein. Outside of this small cluster of residues and the binding region, the AVPI- and AVPF-bound structures overlaid with the AoxSPW-bound structure show about three times as many significant movements (RMSD >∼0.4) compared to the AVPI-bound overlaid with the AVPF-bound structure.

The loss of binding affinity caused by replacing the N-terminal peptide bond with an oxazole ring can be explained by the comparisons made between the peptide-bound and mimic-bound structures. Residues surrounding and distal from the binding site in the protein are relatively more displaced in the AoxSPW-bound structure, which is most likely energetically unfavorable. Some individual interactions between the Smac peptides and the protein, such as hydrogen bonds and hydrophobic contacts, are lost or reduced with AoxSPW. The U-shaped conformation of bound AoxSPW most likely costs entropic energy to adopt. From a rational design

perspective, synthetic modifications to render the U-shaped configuration more energetically favorable would reduce the entropic penalty in adopting such a configuration and could thereby potentially increase binding affinity. For example, the pyrolidine ring could be bridged to the oxazole ring or the indole ring, which would allow the ligand to access the pocket while introducing less conformational strain and possibly gaining some hydrophobic interaction. Also, modifications in the C-terminal portion of the molecule, which have been shown by other studies[15–18] to increase binding affinity, may be adaptable to the oxazole scaffold. Overall, the observations that several BIR3 residues within and surrounding, and distal to the binding site were adjusted to accommodate AoxSPW relative to the tetrapeptides demonstrate the flexibility of the Smac-binding groove in BIR3, and have clear implications in structure function design for the BIR3-XIAP target and in general.

2.5. Cell viability data

In searching for a drug, a primary goal is not only to optimize binding affinity but also to optimize properties that allow for membrane permeability and resistance to degradation in cells or biological fluids. Despite a lower binding affinity, the peptide mimic may display advantages relative to the peptides when assayed in cells, from a presumably better ability to penetrate and/or remain stable in a cellular context. In fact, previous studies which examined the effect of dosing cancer cells with N-terminal Smac peptides showed that, in order to have any effect, the peptides needed to be fused with a cell permeating sequence, such as polyarginine or penetratin.[21–23] In order to assay the ability of the oxazole-containing Smac mimics to enter cells without fusion to a cell-penetrating sequence, cell viability assays were performed. AoxSPW caused a reduction in viability of MBA-MD-231 cells above 30 μM. Despite the higher binding affinity of AVPI, no reduction in cell viability was observed when cells were dosed with up to 500 μM. Relative to cisplatin, higher concentrations of the Smac mimic were required to reduce cell viability (Fig. 4). This result indicates that introduction of the oxazole moiety enabled cellular entry and most likely prevented immediate degradation once inside the cell.

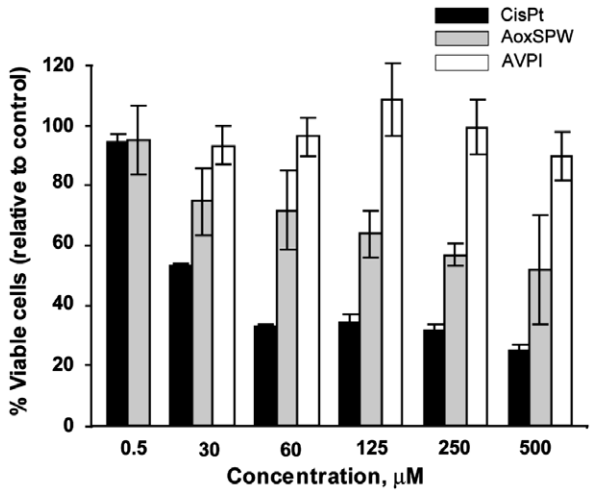

Figure 4. MBA-MD-231 (breast cancer) cells were dosed with cisplatin (black), AoxSPW (gray), AVPI (white), or vehicle at varying concentrations for 72 h. At the end of the dosing period the cell viability was measured using an MTT assay kit and reported relative to control. Standard errors are for three separate experiments run in triplicate (with the exception of the cisplatin which was run once in triplicate).

3. Conclusions

A Smac mimic, AoxSPW, was characterized for binding to BIR3-XIAP biochemically and structurally, and for activity in cancer cells. AoxSPW displayed only moderate affinity for BIR3-XIAP, which was explained by the structural data; however, AoxSPW shows potentially more activity in cells compared to its peptide counterparts and it is the first Smac mimic where the N-terminal peptide bond was replaced. By our results, AoxSPW makes a reasonable scaffold in rational design efforts toward a completely non-peptidic Smac mimic. The scope of this study was to expand the structure activity relationship between the Smac peptides and XIAP to include modification of the N-terminal peptide bond and further synthetic rational design was outside of our aims.

4. Experimental

4.1. Chemistry

All protected amino acids were purchased from Calbiochem-Novabiochem Corp. (San Diego, CA) or Advanced Chemtech (Louisville, KY). HATU and Hünig's base (*N*,*N*-diisopropylethylamine, Biotech grade, 99.5%) were purchased from Aldrich (Milwaukee, WI).

The synthesis of oxazole-containing portion of the peptide mimics has been described previously[24] and is described in Scheme 1. The starting dipeptide (Ala-Ser) was formed by a standard method using the commercially available Ala-succinimide ester (Calbiochem-Novabiochem) with Boc protection on the amine and methyl ester protection on the carboxyl group of Ser (NH2-Ser-OMe, Calbiochem-Novabiochem).

4.1.1. *tert*-Butyl(*S*)-1-(4-(methoxycarbonyl)oxazol-2-ine)ethylcarbamate (2). The oxazoline was synthesized by adding 1.05 equiv of Burgess' reagent ((methyl (carboxysulfamoyl)triethylammonium hydroxide, Aldrich or Acros) in one portion to a stirring solution of the Ala-Ser methyl ester in dry THF under an inert atmosphere. The resulting solution was then heated at 70 °C for ~12 h. The THF was evaporated, the resulting oil was dissolved in EtOAc, and the mixture was washed three times each with 5% (*w*/*v*) aqueous citric acid, saturated aqueous $NaHCO_3$, and brine. The aqueous layers were re-extracted with ethyl acetate and the organic layer was dried with $MgSO_4$. The product was purified by silica gel flash chromatography in 70% ethyl acetate in hexanes. The oxazoline, 2, was formed in 38% yield:

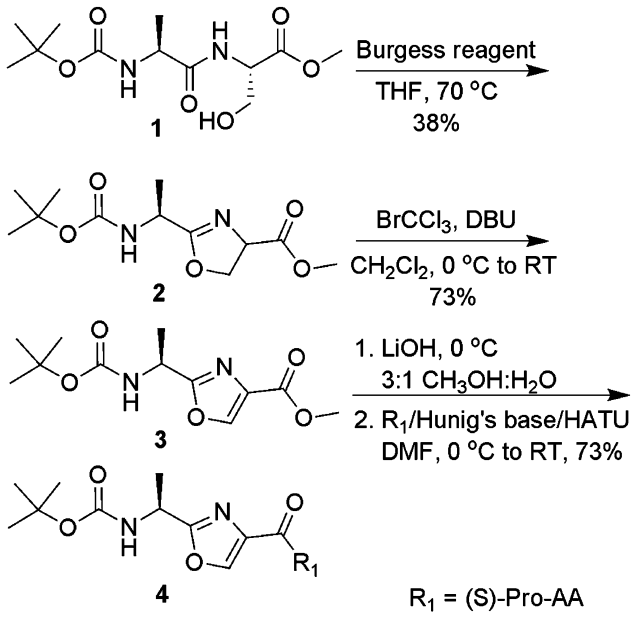

Scheme 1. Synthesis of oxazole containing Smac mimics.[24,25]

R_f = 0.51 (70% EtOAc/hexanes); ^{1}H NMR 400 MHz ($CDCl_3$) δ 1.29–1.46 (s and d overlapping, 12H), 3.69–3.82 (s, 3H), 4.38–4.60 (m, 2H), 4.67–4.79 (m, 1H), 5.15–5.38 (m, 1H).

4.1.2. *tert*-Butyl(*S*)-1-(4-(methoxycarbonyl)oxazol-2-yl)ethylcarbamate (3). The 4,5 oxazoline bond was oxidized with $BrCCl_3$ and DBU (diazobicycloundecane) as base.[25] A solution of 2 in CH_2Cl_2 was cooled to 0 °C and stirred under an inert atmosphere. 1.1 equiv of DBU was added in one portion, then 1.3 equiv $BrCCl_3$ was added dropwise over ~10 min. The mixture was washed twice with aqueous saturated NH_4Cl, the aqueous layer was re-extracted with EtOAc, and the organic layer was dried with $MgSO_4$. The oxazole was purified by silica gel chromatography in 30–50% EtOAc/hexanes. The oxazole, 3, was obtained in 73% yield: R_f: 0.37 (1:1 EtOAc/hex); ^{1}H NMR ($CDCl_3$) d 1.38–1.49 (s, 9H), 1.51–1.58 (d, 3H), 3.87–3.96 (s, 3H), 4.91–5.10 (m, 1H), 5.10–5.31 (m, 1H), 8.12–8.22 (s, 1H).

4.1.3. Coupling of oxazole piece to Pro-X dipeptides. As in Scheme 1, the oxazole piece, 3, was coupled to the Pro-X dipeptide or peptide derivative in a 50–100 mg scale (with respect to the oxazole). The free-acid oxazole was dissolved in a minimum amount of DMF (<5 mL) and brought to 0 °C. 1.4 equiv of HATU and 1 equiv of Hunig's base were added in one portion and the solution was allowed to stir for ~30 min to allow formation of the activated ester. To that solution, the pyrrolidine derivative (free amine, methyl ester) and 2–3 equiv of Hunig's base dissolved in DMF were added. The solution was stirred allowing warming to RT until the reaction was complete. The reaction was worked up by diluting 10-fold with ether, washing five times with saturated NH_4Cl and re-extracting the aqueous layer three to five times. The organic layer was dried with $MgSO_4$. Yields of four ranged from 40% to 80%.

4.1.4. Boc and methyl-ester deprotection methods. Prior to amine deprotection, the methyl ester was stirred at 0 °C in a minimal volume of 3:1 CH_3OH:H_2O. Three equivalents of LiOH was added in one portion. After several hours, the reaction was complete, as indicated by the TLC spot moving to the baseline in 1:10 CH_3OH:$CHCl_3$. The mixture was brought up in EtOAc and washed three times with 5% (*w*/*v*) aqueous citric acid. The aqueous layer was re-extracted three to five times with EtOAc and the combined organic layers were washed once with brine and dried with $MgSO_4$.

To deprotect the amine, a solution of the *tert*-butyl carbamate in CH_2Cl_2 was cooled to 0 °C. Approximately three equivalents of TFA was added in one portion. Upon completion (generally 1–2 h), the reaction mixture was dried by rotoevaporation. The mixture was re-dissolved in CH_2Cl_2 and re-rotoevaporated. This process was repeated three times or until the scent of TFA was no longer detected.

4.1.5. Smac mimic purification and characterization. Smac mimics and peptides were purified by reversed phase HPLC (C18 column, Vydac) or by silica gel chromatography before deprotection and verified on an analytical reversed phase column for purity. The HPLC method used was as follows: Solvent A 99% H_2O, 1% CH_3N, 0.1% TFA, Solvent B 90% CH_3N, 10% H_2O, 0.1% TFA, 10 mL/min (semi-prep) or 1 mL/min (analytical), C_{18} Vydac columns, 230 nm detection, gradient of 1% B/min (0.5%/min analytical), t_0 = 10% B. Smac mimics were dried by lyophilization after purification, collected as TFA salts, and characterized by mass spectroscopy and ^{1}H NMR (400 MHz).

4.1.5.1. NH_2-Ala-oxazole-Pro-Phe-OH (Table 1, entry 1; AoxSPF). *White powder.* ^{1}H NMR (300 MHz, D_2O) δ 1.60, 1.70 (dd, J = 5 Hz, 3H), 1.85–2.25 (m, 3H), 2.90–3.22 (m, 3H), 3.60 (m, 1H), 4.00 (m, 1H), 4.50–4.80 (m, 3H), 5.18 (ad, 1H), 7.18–7.34 (m, 5H), 8.42, 8.45 (ss, 1H). HPLC retention time 32 min (ramp = 1% B/min). MS *m*/*z* 401 $(M+H)^+$. Exact mass ($C_{20}H_{24}O_5N_4$): 400.17442. Mass by HRMS: 400.17442.

4.1.5.2. NH_2-Ala-oxazole-Pro-Trp-OH (Table 1, entry 2; AoxSPW). *Off-white powder.* ^{1}H NMR (400 mMHz. D_2O) δ 1.48,1.52 (dd, J = 6 Hz, 3H), 1.52–2.15 (m, 3H), 2.90–3.41 (m, 3H), 4.05 (q, J = 6 Hz, 1H), 4.20–4.80 (m, 4H), 6.90–7.58 (m, 5H), 8.05, 8.20 (ss, 1H). HPLC retention time 43 min (ramp = 0.5% B/min). Exact mass $(C_{22}H_{26}O_5N_5)^+$: 440.1928. Mass by HRMS: 440.1933.

4.1.5.3. NH_2-Ala-oxazole-Pro-Tyr-OH (Table 1, entry 3; AoxSPY). *White powder.* ^{1}H NMR (400 MHz. D_2O) δ 1.43, 1.56 (dd, J = 7 Hz, 3H), 1.62–1.82 (m, 2H), 1.97–2.15 (m, 1H), 2.62–3.08 (m, 3H), 3.45 (m, 1H), 3.78 (ad, 1H), 4.38–4.45 (m, 2H), 4.85 (ad, 1H), 6.68 (dd, J = 4.7 Hz, 2H), 6.96 (dd, J = 8.25 Hz, 2H), 8.05, 8.20 (ss, 1H). HPLC retention time 24 min (ramp = 0.5% B/min). MS *m*/*z* 418 $(M+H)^+$. Exact mass ($C_{20}H_{24}N_4O_6$): 416.16958. Mass by HRMS: 416.16818.

4.1.5.4. NH_2-Ala-oxazole-Pro-Ile-OH (Table 1, entry 4; AoxSPI). *Off-white crystalline solid.* ^{1}H NMR δ (400 MHz, D_2O) δ 0.68–0.83 (m, 6H), 0.94–1.38 (m, 1H), 1.52, 1.58 (dd, J = 8 Hz, 3H), 1.60–2.25 (m, 4H), 3.75 (m, 1H),), 3.42–3.60 (m, 1H), 3.98, 4.14 (dd, J = 6 Hz, 1H), 4.45 (m, 1H), 5.04 (m, 1H), 8.22, 8.24 (ss, 1H). HPLC retention time 40 min (ramp = 0.5% B/min). MS m/z 367 $(M+H)^+$. Exact mass ($C_{17}H_{26}N_4O_5$): 366.19032. Mass by HRMS: 366.18863.

4.2. Binding assay conditions

Before the compounds were assayed, the solid was brought up in D_2O and the concentration was measured by ^{1}H NMR with an internal dioxane reference of known concentration. The assay is a competitive fluorescent-binding assay described previously.[19] Briefly, the dye is comprised of a Smac peptide (AVPC) conjugated to a fluorescent dye, BADAN (Molecular Probes, Invitrogen Corp., Carlsbad, CA) through a thiol-ester linkage at Cys. When the dye is bound to BIR-XIAP, the fluorescence emission (centered at 550 nm) is of higher intensity and a second peak appears centered at 470 nm. As the dye is displaced from the protein by a competing peptide or peptide mimic the fluorescence emission is reduced and resembles that of the AVPC-badan dye in solution alone. The AUC for the emission spectra of AVPC-badan alone, AVPC-badan, and for the Smac mimic bound to BIR3-XIAP are used to calculate a relative K_D for the Smac mimic. The relative K_D is then converted to an absolute K_D using the K_D value for AVPC-badan, which was determined in titration assay.[19]

4.3. Crystallization and data collection

Crystals were grown by the hanging-drop vapor-diffusion method by mixing an equal volume of reservoir solution. The reservoir contained 0.1 M Hepes, pH 7.5, and 4.3 M NaCl for AoxSPW with BIR3-XIAP and 0.1 M MES, pH 6.5; 1.6 M magnesium sulfate heptahydrate for AVPF with BIR3-XIAP. The BIR3-XIAP constructs included residues 249–354 for AoxSPW and 249–357 for AVPF. The peptide or Smac mimic was co-crystallized with the protein in 10:1 molar excess of AVPF to BIR3-XIAP or 25:1 molar excess of AoxSPW to BIR3-XIAP. Cryobuffer was the same as the reservoir buffer but contained 10–15% glycerol. The crystallographic data and refinement statistics are shown in Table 2 for AoxSPW:BIR3 and in Table 3 for AVPF:-BIR3. The structures can be found in the Protein Data Bank (PDBID 2OPY AoxSPW:BIR3 and 2OPZ AVPF:BIR3).

4.4. Cell culture and MTT assay

MBA-MD-231 cell line was purchased from the ATCC (American Type Culture Collection). The cells are cultured in DMEM containing 10% fetal bovine serum, penicillin, and streptomycin at the recommended doses and stored in humidified incubators regulated at 37 °C and 5% CO_2. Cells are passed by trypsination once every 5–7 days.

Table 2. Data collection and statistics from crystallographic analysis of AoxSPW bound to BIR3-XIAP

Data set	
Space group	P4122
Unit cell dimension	71.2, 71.2, 105.1, 90.0, 90.0, 90.0
Resolution (Å)	20–2.8
Total observations	215,384
Unique observations	7126
Data coverage (outer shell)	99.9%(100%)
R_{sym} (outer shell)	0.076(0.447)
Refinement	
Resolution (Å)	20–2.8
R (R_{free})	0.213 (0.235)
Rmsd bonds	0.007
Rmsd angles	1.34
Total number of reflections used	6878
Working set	6502
Test set	376
Solvent	75.00%
Water molecules	64

Zn-MAD data sets were collected at the Brookhaven National Laboratory.
$R_{sym} = \Sigma_h\Sigma_i|I_{h,i} - I_h|/\Sigma_h\Sigma_i I_{h,i}$, where I_h is the mean intensity of the i observations of symmetry related reflections of h. $R = \sum|F_{obs} - F_{calc}|/\sum F_{obs}$, where $F_{obs} = F_P$, and F_{calc} is the calculated protein structure factor from the atomic model (R_{free} was calculated with 5% of the reflections). Rmsd in bond lengths and angles are the deviations from ideal values, and the rmsd deviation in B factors is calculated between bonded atoms.

Table 3. Data collection and statistics from crystallographic analysis of AVPF bound to BIR3-XIAP

Data set	
Space group	$I2_13$
Unit cell dimension	170.4, 170.4, 170.4, 90.0, 90.0, 90.0
Resolution (Å)	50–3.0
Total observations	276,259
Unique observations	15,951
Refinement	
Resolution(Å)	500.0–3.0
R (R_{free})	0.231 (0.277)
Rmsd bonds	0.011326
Rmsd angles	1.78703
Total number of reflections used	15951
Working set	14352
Test set	1599

Data sets were collected at the Brookhaven National Laboratory.
$R_{sym} = \Sigma_h\Sigma_i|I_{h,i} - I_h|/\Sigma_h\Sigma_i I_{h,i}$, where I_h is the mean intensity of the i observations of symmetry related reflections of h. $R = \sum|F_{obs} - F_{calc}|/\sum F_{obs}$, where $F_{obs} = F_P$, and F_{calc} is the calculated protein structure factor from the atomic model (R_{free} was calculated with 5% of the reflections). Rmsd in bond lengths and angles are the deviations from ideal values, and the rmsd deviation in B factors is calculated between bonded atoms.

The compound to be tested was dissolved in DMSO at 100 times the highest concentration to be tested. A 1:50 dilution into cellular medium (phenol red-free DMEM, no antibiotic, 10% fetal bovine serum) was made to yield a solution that is twice the highest test dose and 2% DMSO. The dose solution was pipetted into a tissue culture treated 96-well plate, n = 3 for each

concentration. Serial 1:2 dilutions were made with cellular medium containing 2% DMSO. The cells were trypsinized, reconstituted in the cellular medium (DMSO free), and counted using a hemacytometer. If necessary, appropriate dilutions were made so that the concentration became 1×10^5 cells/mL. Fifty microliters of cell suspension was added to each well (1:2 dilution was made when cells are added to each well). The dosed cells are incubated for 72 h. The MTT assay (Promega, G4000) protocol is followed to obtain cell viability data. The assay was repeated three times for each cell line assayed.

Acknowledgments

The authors acknowledge Dr. E. Shiozaki for assistance with early crystallographic work. Dr. M. Semmelhack and Dr. M. Zhou for indispensable advice and critical reading of the manuscript. Dr. I. Pelczer for assistance with NMR spectroscopy, and Drs. D. Little and J. Eng for mass spectroscopy.

References and notes

1. Green, D. R.; Reed, J. C. *Science* **1998**, *281*, 1309–1312.
2. Shi, Y. G. *Nat. Struct. Biol.* **2001**, *8*, 394–401.
3. Thompson, C. B. *Science.* **1995**, *267*, 1456–1462.
4. Deveraux, Q. L.; Reed, T. C. *Gene Dev.* **1999**, *13*, 239–252.
5. LaCasse, E. C.; Baird, S.; Korneluk, R. G.; MacKenzie, A. E. *Oncogene* **1998**, *17*, 3247–3259.
6. Du, C. Y.; Fang, M.; Li, Y. C.; Li, L.; Wang, X. D. *Cell* **2000**, *102*, 33–42.
7. Verhagen, A. M.; Ekert, P. G.; Pakusch, M.; Silke, J.; Connolly, L. M.; Reid, G. E.; Moritz, R. L.; Simpson, R. J.; Vaux, D. L. *Cell* **2000**, *102*, 43–53.
8. Ekert, P. G.; Silke, J.; Hawkins, C. J.; Verhagen, A. M.; Vaux, D. L. *J. Cell Biol.* **2001**, *152*, 483–490.
9. Srinivasula, S. M.; Hegde, R.; Saleh, A.; Datta, P.; Shiozaki, E.; Chai, J. J.; Lee, R. A.; Robbins, P. D.; Fernandes-Alnemri, T.; Shi, Y. G.; Alnemri, E. S. *Nat. Struct. Biol.* **2001**, *410*, 112–116.
10. Tamm, I.; Kornblau, S. M.; Segall, H.; Krajewski, S.; Welsh, K.; Kitada, S.; Scudiero, D. A.; Tudor, G.; Qui, Y. H.; Monks, A.; Andreeff, M.; Reed, J. C. *Clin. Cancer Res.* **2000**, *6*, 1796–1803.
11. Archakov, A. I.; Govorun, V. M.; Dubanov, A. V.; Ivanov, Y. D.; Veselovsky, A. V.; Lewi, P.; Janssen, P. *Proteomics* **2003**, *3*, 380–391.
12. Schade, M.; Oschkinat, H. *Curr. Opin. Drug Discovery Dev.* **2005**, *8*, 365–373.
13. Liu, Z. H.; Sun, C. H.; Olejniczak, E. T.; Meadows, R. P.; Betz, S. F.; Oost, T.; Herrmann, J.; Wu, J. C.; Fesik, S. W. *Nat. Struct. Biol.* **2000**, *408*, 1004–1008.
14. Wu, G.; Chai, J. J.; Suber, T. L.; Wu, J. W.; Du, C. Y.; Wang, X. D.; Shi, Y. G. *Nat. Struct. Biol.* **2000**, *408*, 1008–1012.
15. Oost, T. K.; Sun, C. H.; Armstrong, R. C.; Al-Assaad, A. S.; Betz, S. F.; Deckwerth, T. L.; Ding, H.; Elmore, S. W.; Olejniczak, E. T.; Oleksijew, A.; Oltersdorf, T.; Rosenberg, S. H.; Shoemaker, A. R.; Tomaselli, K. J.; Zou, H.; Fesik, S. W. *J. Med. Chem.* **2004**, *47*, 4417–4426.
16. Li, L.; Thomas, R. M.; Suzuki, H.; De Brabander, J. K.; Wang, X.; Harran, P. G. *Science* **2004**, *305*, 1471–1474.
17. Sun, H.; Nikolovska-Coleska, Z.; Yang, C. Y.; Xu, L.; Liu, M.; Tomita, Y.; Pan, H.; Yoshioka, Y.; Krajewski, K.; Roller, P. P.; Wang, S. *J. Am. Chem. Soc.* **2004**, *2004*, 51.
18. Zobel, K.; Wang, L.; Varfolomeev, E.; Franklin, M. C.; Elliott, L. O.; Wallweber, H. J. A.; Okawa, D. C.; Flygare, J. A.; Vucic, D.; Fairbrother, W. J.; Deshayes, K. *ACS Chem. Biol.* **2006**, *1*, 525–533.
19. Kipp, R. A.; Case, M. A.; Wist, A. D.; Cresson, C. M.; Carrell, M.; Griner, E.; Wiita, A.; Albiniak, P. A.; Chai, J. J.; Shi, Y. G.; Semmelhack, M. F.; McLendon, G. L. *Biochemistry* **2002**, *41*, 7344–7349.
20. DeLano, W. The PyMol Molecular Graphics System. DeLano Scientific LLC: San Carlos, CA, USA, <http://www.pymol.org.>.
21. Arnt, C. R.; Chiorean, M. V.; Heldebrant, M. V.; Gores, G. J.; Kaufmann, S. H. *J. Biol. Chem.* **2002**, *277*, 44236–44243.
22. Fulda, S.; Wick, W.; Weller, M.; Debatin, K. M. *Nat. Med.* **2002**, *8*, 808–815.
23. Yang, L. L.; Mashima, T.; Sato, S.; Mochizuki, M.; Sakamoto, H.; Yamori, T.; Oh-hara, T.; Tsuruo, T. *Cancer Res.* **2003**, *63*, 831–837.
24. Wipf, P.; Miller, C. P. *Tetrahedron Lett.* **1992**, *33*, 907–910.
25. Williams, D. R.; Lowder, P. D.; Gu, Y.; Brooks, D. A. *Tetrahedron Lett.* **1997**, *38*, 331–334.